A decomposition method for directional Total Variation with application to needle reconstruction in interventional imaging

Marion Savanier, Cyril Riddell, Yves Trousset, Emilie Chouzenoux, Jean-Christophe Pesquet

A decomposition method for directional Total Variation with application to needle reconstruction in interventional imaging

Marion Savanier[a,b], Cyril Riddell[a], Yves Trousset[a], Emilie Chouzenoux[b], and Jean-Christophe Pesquet[b]

[a]GE Healthcare, Buc, France
[b]Université Paris-Saclay, CentraleSupélec, Centre pour la Vision Numérique, Inria, Gif-sur-Yvette

ABSTRACT

In interventional radiology, 3D reconstruction of devices such as needles can increase the precision of procedures. Doing so with CBCT is time-consuming and increases the X-ray dose. Needles being sparse, a compressed-sensing reconstruction approach seems viable. In this paper, we thus investigate the benefits of directional total variation as an adequate prior for anisotropic devices. We introduce a decomposition method that allows several a priori directions to be considered at once as well as excludes the anatomical background that is not sparse. The capacity of the method is illustrated in simulations of limited-angle acquisitions. It allows good reconstruction of the needles from a small angular coverage, even if the anatomical background cannot be recovered.

Keywords: CT, directional total variation, limited-angle reconstruction, optimization-based reconstruction

1. INTRODUCTION

Flat-panel C-arm systems provide real-time 2D imaging to guide the navigation of therapeutic devices during minimally invasive vascular or percutaneous procedures. In the following, we shall focus on interventions using metallic needles, such as vertebroplasty, radiofrequency ablations, or biopsies. Cone-beam computed tomography (CBCT) is available through the rotation of the C-arm around the patient. It allows the 3D reconstruction of highly attenuating metallic devices together with the patient background anatomy. In the guidance phase of the procedure, the patient is positioned to optimize the real-time visualization of the device and its trajectory. Although a CBCT scan could be performed to precisely assess the position of the device according to the planned trajectory, repeated acquisitions increase the X-ray dose received by the patient. Furthermore, the patient may need to be moved to another position to avoid collisions during the 200° rotation required by tomography. Rotating over a smaller angular coverage would reduce the number of times changing the position of the patient is needed and would reduce the number of projections and the amount of X-ray dose. Model-based iterative reconstruction methods (MBIR) have proven useful in reconstructing soft tissues from a reduced number of projections over a full tomographic angular coverage. In Ref.,[1] a least-squares criterion regularized with total variation (TV) was used to remove the under-sampling streaks of dense objects over the less dense soft tissues. However, TV regularization is isotropic: in 2D, it penalizes the ℓ_1 norm of the image partial derivatives along the vertical and horizontal directions equally. TV cannot recover the edges along directions not sampled by the limited angular coverage. Only edges and details tangent to the projection directions are recovered.[2] For piecewise constant geometrical objects, successful results have been obtained with the anisotropic total variation (ATV). ATV assigns different weights to the vertical and horizontal partial derivatives of the image. This strategy allows for considering the angular range as an additional prior information.[3] Since the non-convex ℓ_0 pseudo-norm is the most direct measure of the sparsity of an object, ℓ_1-reweighting strategies and heuristics have been investigated to incorporate the idea of independence on the magnitude of the ℓ_0-norm into the ATV approach. However, due to non-convexity, it is not clear that the resulting optimization methods converge to a global minimum.[3–5] Recently, ATV-constrained formulations (instead of regularization-based ones) allowed for

Further author information: (Send correspondence to C. Riddell)
E-mail: Cyril.Riddell@med.ge.com

reconstructing complex patterns from limited angle acquisitions.[6] The anisotropic regularizer proposed in Ref.[7] is particularly suited to thin objects like needles because it emphasizes one specific direction. In the following, we call it directional total variation (DTV). DTV relies on estimating the gradient norm along one selected direction that is not necessarily aligned with the pixel grid. Applications on denoising and reconstructing images of fiber materials have been successful.[8] Additionally, DTV with a spatially varying direction and strength,[9–11] that includes higher order derivatives[8,12] has been proposed to extend the applicability of DTV, for instance, to vessels and fingerprints. In this work, we consider the simple geometric shape of needles that is very sparse and can be reconstructed from a limited-angle acquisition. However, we here allow more directions than one and superimpose them over a non-sparse anatomical background. We adopt an image decomposition approach that applies DTV over multiple directions for the needles and TV to approximate the background. Decomposition was first proposed for texture-geometry decomposition[13] and has also been applied to CT imaging to decompose the reconstruction into three components of the object, sub-sampling artifacts and noise.[14]
In Section 2, we review the DTV regularization for incorporating directional information and the decomposition method to selectively apply separate directional constraints on separate components and exclude the anatomical background. Numerical experiments are then provided and discussed in Section 3 to illustrate the potential of the proposed method.

2. METHOD

2.1 Scanning model

Data collected in X-ray tomographic imaging can be modeled by the following discrete linear system

$$\mathbf{y} = \mathbf{H}\mathbf{x} + \mathbf{b} \tag{1}$$

where $\mathbf{H} \in \mathbb{R}^{M\times N}$ is the discretized model of forward projection,[15] $\mathbf{x} \in \mathbb{R}^N$ is the unknown attenuation image, $\mathbf{y} \in \mathbb{R}^M$ represents the log-transform of the data measured by the detector and $\mathbf{b} \in \mathbb{R}^M$ is an additive noise term.
In a limited angle setting, (1) is a severely under-determined system of linear equations. The lack of data must be compensated by a priori knowledge that constrains the problem by limiting the space of feasible solutions. To estimate $\mathbf{x}$, we consider the sum of a least-squares data fidelity term and a convex regularizer g embedding this prior information, in particular, sparsity and direction:

$$\underset{\mathbf{x}\in\mathbb{R}^N}{\text{minimize}} \;\; \frac{1}{2}\|\mathbf{y}-\mathbf{H}\mathbf{x}\|_{\mathbf{D}}^2 + g(\mathbf{x}). \tag{2}$$

Matrix $\mathbf{D}$ is symmetric positive definite. We now discuss the choices for g.

2.2 Directional total variation (DTV)

DTV enforces the prior that the object is piecewise constant and follows one main direction. For an image $\mathbf{x} \in \mathbb{R}^N$, its DTV can be defined as $\mathrm{DTV}_\Omega(\mathbf{x}) = \sum_{n=1}^N \|(\nabla_\Omega \mathbf{x})_n\|_1 = \|\Lambda \mathbf{R}_\theta(\nabla \mathbf{x})\|_{1,1}$ where $\Omega = \{\theta, s\}$, $\nabla_\Omega \in \mathbb{R}^{2\times N}$ contains two directional derivatives at pixel n, $\Delta_n^\theta \mathbf{x}$ and $\Delta_n^{\theta+\pi/2}\mathbf{x}$, parameterized by direction angle $\theta \in [0°, 180°[$, and a "stretching factor" $s \in]0, 1]$ for anisotropy, i.e.

$$\begin{aligned}(\nabla_\Omega \mathbf{x})_n &= \begin{pmatrix} \Delta_n^\theta \mathbf{x} \\ s\Delta_n^{\theta+\pi/2}\mathbf{x} \end{pmatrix} = \Lambda \mathbf{R}_\theta \begin{pmatrix} \Delta_n^{\mathrm{h}} \mathbf{x} \\ \Delta_n^{\mathrm{v}} \mathbf{x} \end{pmatrix} \\ &= \begin{pmatrix} 1 & 0 \\ 0 & s \end{pmatrix} \begin{pmatrix} \cos\theta & \sin\theta \\ -\sin\theta & \cos\theta \end{pmatrix} \begin{pmatrix} \Delta_n^{\mathrm{h}} \mathbf{x} \\ \Delta_n^{\mathrm{v}} \mathbf{x} \end{pmatrix},\end{aligned} \tag{3}$$

with $\Delta_n^{\mathrm{h}} \in \mathbb{R}^N$, $\Delta_n^{\mathrm{v}} \in \mathbb{R}^N$, respectively, the horizontal and vertical discrete gradient operators at location n. These quantities can be obtained by applying a forward finite difference scheme with zero boundary conditions. Given that a set of needles makes a very sparse image, we add an ℓ_1 penalty so that $g(\mathbf{x}) = g_\Omega(\mathbf{x}) = \rho \mathrm{DTV}_\Omega(\mathbf{x}) + \alpha\|\mathbf{x}\|_1$, $(\alpha, \rho) \in]0, +\infty[^2$ in (2).

2.3 Image decomposition

With a non-sparse background, the lack of data cannot be compensated, and the problem does not have a sparse solution. Decomposing $\mathbf{x}$ into a linear combination of several components aims to restore sparsity in all components that can then be recovered from the limited data. A component is thus defined by its specific sparsity prior. A different sparse approximation is used to direct the interfering background into a single component. Then instead of estimating the sum directly, we solve the minimization problem for each component simultaneously. Here we decompose $\mathbf{x}$ into the anatomical background component $\mathbf{x}_{\mathrm{B}}$ penalized with TV and $I \in \mathbb{N}$ directional components $\mathbf{x}_{\Omega_i}$ penalized with DTV of direction $\theta_i \in [0°, 180°[$ and stretching parameter $s_i \in]0, +\infty[$ such that

$$\mathbf{x} = \mathbf{x}_{\mathrm{B}} + \sum_{i=1}^{I} \mathbf{x}_{\Omega_i} \tag{4}$$

where $\Omega_i = \{\theta_i, s_i\}$, $i \in \{1, \dots, I\}$.
Altogether, we must solve the following convex problem:

$$\underset{\mathbf{x}_{\mathrm{B}}, (\mathbf{x}_{\Omega_i})_{i=1}^{I} \in \mathbb{R}^N}{\text{minimize}} \ \frac{1}{2}\|\mathbf{y} - \mathbf{H}(\mathbf{x}_{\mathrm{B}} + \sum_{i=1}^{I} \mathbf{x}_{\Omega_i})\|_{\mathbf{D}}^2 + \sum_{i=1}^{I} g_{\Omega_i}(\mathbf{x}_{\Omega_i}) + g_{\mathrm{TV}}(\mathbf{x}_{\mathrm{B}}).$$

where $g_{\mathrm{TV}}(\mathbf{x}_{\mathrm{B}}) = \beta\|\nabla \mathbf{x}_{\mathrm{B}}\|_{1,2}$, $\beta \in]0, +\infty[+ i_{[0,+\infty[^T}(\mathbf{x}_{\mathrm{B}})$.
Note that each directional component $\mathbf{x}_{\Omega_i}$ can capture a needle or a group of needles following about the same direction.

2.4 Optimization algorithm

To minimize Problem (5), we reformulate it. Let $\mathbf{z} = \begin{bmatrix} \mathbf{x}_{\mathrm{B}}^\top & \mathbf{x}_{\Omega_1}^\top & \dots & \mathbf{x}_{\Omega_I}^\top \end{bmatrix}^\top \in \mathbb{R}^{(I+1)N}$. Let $\tilde{\mathbf{H}} = \Pi\mathbf{H}$ and $\tilde{\mathbf{D}} = \Pi\mathbf{D}$ where $\Pi \colon \mathbf{M} \mapsto \begin{bmatrix} \mathbf{M} & \dots & \mathbf{M} \end{bmatrix} \in \mathbb{R}^{((I+1)L)\times L}$. We then write:

$$\underset{\mathbf{z} \in \mathbb{R}^{(I+1)N}}{\text{minimize}} \ \frac{1}{2}\|\mathbf{y} - \tilde{\mathbf{H}}\mathbf{z}\|_{\tilde{\mathbf{D}}}^2 + h(\mathbf{z}), \tag{5}$$

with $h \colon \mathbf{z} \mapsto \sum_i^I g_{\Omega_i}(\mathbf{x}_{\Omega_i}) + g_{\mathrm{TV}}(\mathbf{x}_{\mathrm{B}})$.
The cost function in Equation (5) is convex but non-smooth. In this context, FISTA algorithm[16] is attractive due to its simplicity and low-memory requirements. It relies on the use of proximal operators. Let us recall that the proximity operator of h at $\mathbf{x}$ is defined as $\mathrm{prox}_h(\mathbf{x}) = \underset{\mathbf{z} \in \mathbb{R}^N}{\operatorname{argmin}} \ \left(h(\mathbf{z}) + \frac{1}{2}\|\mathbf{x} - \mathbf{z}\|^2\right)$.
Let a be a positive real number such that $a > 2$. The k-th iteration of FISTA applied to Problem (5) reads:

$$\begin{cases} \beta_k = k/(k+1+a) \\ \tilde{\mathbf{z}}^k = \mathbf{z}^k + \beta_k(\mathbf{z}^k - \mathbf{z}^{k-1}) \\ \mathbf{z}^{k+1} = \mathrm{prox}_{\tau h}(\tilde{\mathbf{z}}^k - \tau\tilde{\mathbf{H}}^\top\tilde{\mathbf{D}}(\mathbf{H}\tilde{\mathbf{z}}^k - \mathbf{y})) \end{cases} \tag{6}$$

where $z^0 \in \mathbb{R}^{(I+1)N}$.
Thanks to the separability in each component of $\mathbf{z}$, we derive an update rule for each map:

$$\begin{cases} \beta_k = k/(k+1+a) \\ \tilde{\mathbf{x}}_{\mathrm{B}}^k = \mathbf{x}_{\mathrm{B}}^k + \beta_k(\mathbf{x}_{\mathrm{B}}^k - \mathbf{x}_{\mathrm{B}}^{k-1}) \\ \text{For } i \in \{1, \dots, I\}\text{:} \\ \quad \tilde{\mathbf{x}}_{\Omega_i}^k = \mathbf{x}_{\Omega_i}^k + \beta_k(\mathbf{x}_{\Omega_i}^k - \mathbf{x}_{\Omega_i}^{k-1}) \\ \mathbf{x}^k = \tilde{\mathbf{x}}_{\mathrm{B}}^k + \sum_i^I \tilde{\mathbf{x}}_i^k \\ \mathbf{x}_{\mathrm{B}}^{k+1} = \mathrm{prox}_{\tau g_{\mathrm{TV}}}(\tilde{\mathbf{x}}_{\mathrm{B}}^k - \tau\mathbf{H}^\top\mathbf{D}(\mathbf{H}\mathbf{x}^k - \mathbf{y})) \\ \text{For } i \in \{1, \dots, I\}\text{:} \\ \quad \mathbf{x}_{\Omega_i}^{k+1} = \mathrm{prox}_{\tau g_{\Omega_i}}(\tilde{\mathbf{x}}_{\Omega_i}^k - \tau\mathbf{H}^\top\mathbf{D}(\mathbf{H}\mathbf{x}^k - \mathbf{y})) \end{cases} \tag{7}$$

The convergence of Algorithm 7 is guaranteed for $0 < \tau \leqslant 1/|||\tilde{\mathbf{H}}^\top \tilde{\mathbf{D}}\tilde{\mathbf{H}}||| = 1/(I+1)|||\mathbf{H}^\top \mathbf{D}\mathbf{H}|||$ where $|||\cdot|||$ denotes the spectral norm of the input matrix.
The proximity operators of $\mathbf{x} \mapsto \tau g_{\mathrm{TV}}(\mathbf{x})$ and $\mathbf{x} \mapsto \tau g_{\Omega_i}(\mathbf{x})$ do not have a closed form; hence they are both approximated by using inner iterations of the dual forward-backward (DFB) algorithm[17] with warm-restart. In particular, for DTV, $\hat{\mathbf{x}} = \mathrm{prox}_{\tau g_{\Omega_i}}(\tilde{\mathbf{x}})$ is estimated using the following sub-iteration:

$$\begin{cases} \mathbf{x}^n = \mathrm{proj}_{[0,+\infty[^N}(\tilde{\mathbf{x}} - \nabla_\Omega^\top \mathbf{u}^n) \\ \mathbf{u}^{n+1} = \mathrm{proj}_{\|\cdot\|_{\infty,\infty} \leqslant \tau\rho}(u_n + \gamma \nabla_\Omega \mathbf{x}^n) \end{cases} \tag{8}$$

where $\gamma < 2/|||\nabla_\Omega|||^2$, $\mathbf{u}^0 \in \mathbb{R}^{2N}$ and $\|\mathbf{u}^n\|_{\infty,\infty}$ is the maximum value of the 2 components of $\mathbf{u}^n \in \mathbb{R}^{2N}$.

3. EXPERIMENTS

3.1 Simulations

We carry out simulations in parallel geometry using two numerical phantoms on a 256×256 grid. Hounsfield units (HU) are shifted such that air has value 0 HU and water is 1000 HU. Phantom (A) is purely geometric and represents a set of needles of intensity 3500 HU covering 8 directions (5°, 27.5°, 50°, 72.5°, 95°, 107.5°, 130°, 152.5°) as shown in Figure 1 (angles start at twelve o'clock and grow clockwise). Phantom (B) is the sum of an axial CT slice of an abdomen (see Figure 1) with a subset of needles of varying intensity (3000-5000 HU).
A needle is within the scanning arc if the projection data contain its so-called bull's eye view, i.e., the view orthogonal to its axis. We computed simulated data of these phantoms over a circular arc of amplitude $\nu = 66°$ from angle $\theta_{\min} = 29°$ to angle $\theta_{\max} = 95°$ (indicated by the arrows in Figure 1) so that the projection data contained the bull's eye view of three needles. Noise term $\mathbf{b}$ was i.i.d. Gaussian of mean 0 and standard deviation 50. The angular sampling was uniform with a step of 2°. Reconstruction with TV regularization was taken as a baseline. FBP reconstruction followed by thresholding of the intensity was added to the comparison. We performed 100 iterations of DFB and 5000 iterations of FISTA.
First, we analyzed the performance of our decomposition method (5) for the reconstruction of a subset of the needles of Phantom (A) thanks to four DTV of direction $\{5°, 27.5°, 72.5°, 107.5°\}$ (i.e., $I = 4$). Then we showed the method's applicability to the more complex case of a background and needles of different intensities by reconstructing Phantom (B). This time, a set of $I = 3$ directions was used: $\{27.5°, 72.5°, 107.5°\}$. In all these simulations, the needles have the same size, so we used the same stretching parameter $s = 0.001$. Needles with the same intensity have the same regularization parameters ρ and α. Matrix $\mathbf{D}$ was chosen as the ramp filter which provides an approximate inversion of $\mathbf{H}\mathbf{H}^\top$.[1] The TV and DTV parameters then became thresholds that are homogeneous to the HU intensity values of the image.

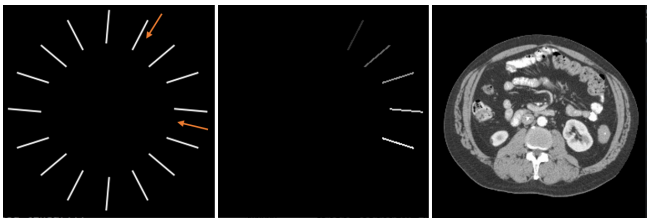

Figure 1. Reference images. From left to right: Phantom (A) with needles of intensity 3500 HU, Image with needles of growing intensity from 3000 HU up to 5000 HU, Anatomical background [1800-2200 HU].

3.2 Background-free needles

Figure 2 shows the reconstructions of Phantom (A) with FBP, TV ($\beta = 50$) and DTV ($\rho = 50$, $\alpha = 1$). First, we see that with FBP, only partial reconstruction of the three needles within the scanning arc is achieved. Figure 3 displays the four reconstructed directional components. Both DTV and TV regularization lead to similar reconstructions for the three needles in the scanning arc. For the two needles of direction close to $\theta_{\min}$, TV yielded a partial recovery only, whereas DTV fully recovered 12 out of 16 needles because their directions were sufficiently close to the imposed a priori directions. The four remaining missing needles show that there is no recovery without a priori directional information.

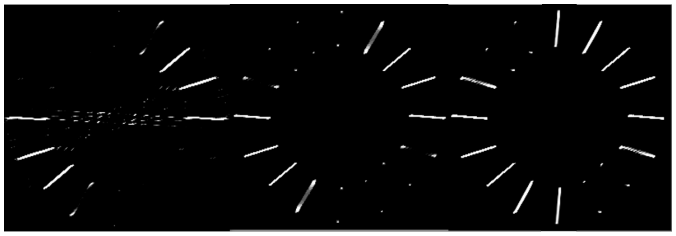

Figure 2. Reconstructed images for $\nu = 66°$. From left to right: FBP, TV, DTV.

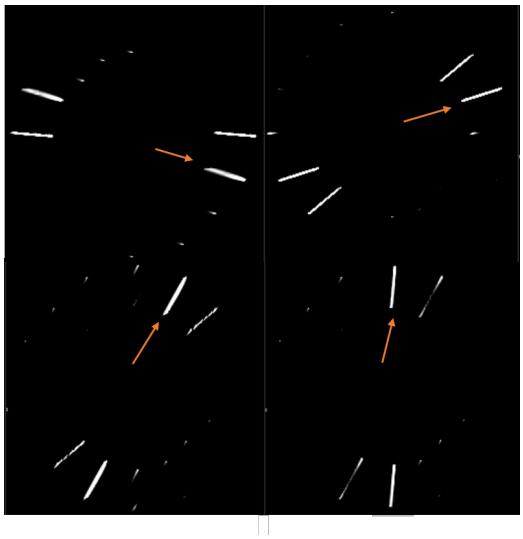

Figure 3. Directional components obtained with DTV model on Phantom (A). Top: from left to right, $\theta_1 = 107.5°$, $\theta_2 = 72.5°$. Bottom: from left to right, $\theta_3 = 27.5°$, $\theta_4 = 5°$.

3.3 Needles with background

Figure 5 shows the reconstruction of the needles of Phantom (B) with FBP, TV, and DTV (sum of all needle maps). First, as expected, the anatomical background cannot be recovered with a sparse prior in this limited angle setting. The needles reconstructed with FBP are distorted, and the intensity values are not recovered. With TV, only the three needles within the scanning arc remain after thresholding, whereas five needles are recovered with DTV. Figure 4 shows that the decomposition method coupled with directional information separates the three sets of needles from the background map.

Figure 4. Reconstructed needles maps obtained with DTV model on Phantom (B). From left to right: $\mathbf{x}_{\Omega_1}$ ($\theta_1 = 107.5°$), $\mathbf{x}_{\Omega_2}$ ($\theta_2 = 27.5°$), $\mathbf{x}_{\Omega_3}$ ($\theta_3 = 72.5°$).

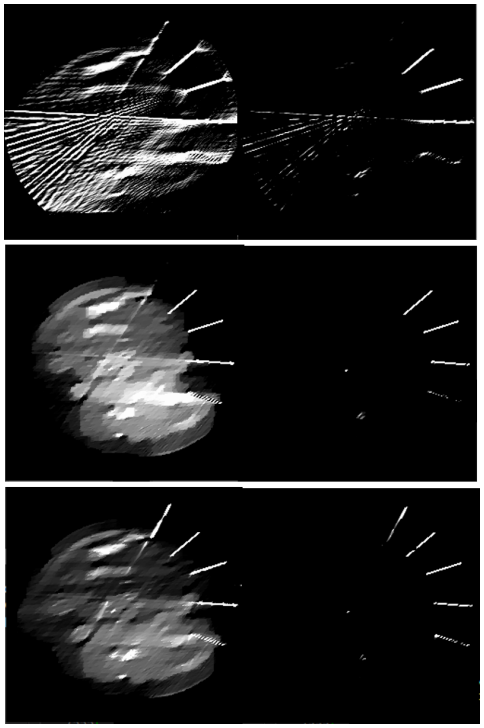

Figure 5. Reconstruction of needles of Phantom (B) in the presence of a background for $\nu = 66°$. Left: needles with background. Right: needles map. From top to bottom: FBP, TV, DTV.

4. DISCUSSION AND CONCLUSION

In this paper, we exploited the simple geometric shape of percutaneous needles, which is very sparse and follows one main direction for iterative reconstruction. We introduced a decomposition method that allows several DTV regularizations - and thus several directional a priori to be considered at once - and treats the anatomical background separately. The potential of our DTV decomposition method for reconstructing geometrical objects from small scanning arcs was confirmed in our results, where needles are recovered even when their bull's eye view is not sampled. This approach is promising for increasing the precision of interventional radiology procedures through limited-angle acquisitions. Our study is, however, limited to background interference, as it is based on nearly perfect data. Data corruption due to physical effects and stronger noise, particularly metallic artifacts, is another source of interference that may limit the capacity of sparse priors and must be dealt with before clinical application.

REFERENCES

[1] Langet, H., Riddell, C., Reshef, A., Trousset, Y., Tenenhaus, A., Lahalle, E., Fleury, G., and Paragios, N., "Compressed-sensing-based content-driven hierarchical reconstruction: Theory and application to C-arm cone-beam tomography," *Medical Physics* **42**(9), 5222–5237 (2015).

[2] Quinto, E. T., "Tomographic reconstructions from incomplete data numerical inversion of the exterior radon transform," *Inverse Problems* **4**(3), 867 (1988).

[3] Wang, T., Nakamoto, K., Zhang, H., and Liu, H., "Reweighted anisotropic total variation minimization for limited-angle ct reconstruction," *IEEE Transactions on Nuclear Science* **64**(10), 2742–2760 (2017).

[4] Yu, W., Wang, C., and Huang, M., "Edge-preserving reconstruction from sparse projections of limited-angle computed tomography using ℓ_0-regularized gradient prior," *Review of Scientific Instruments* **88**(4), 043703 (2017).

[5] Xu, J., Zhao, Y., Li, H., and Zhang, P., "An image reconstruction model regularized by edge-preserving diffusion and smoothing for limited-angle computed tomography," *Inverse Problems* **35**(8), 085004 (2019).

[6] Zhang, Z., Chen, B., Xia, D., Sidky, E. Y., and Pan, X., "Directional-tv algorithm for image reconstruction from limited-angular-range data," *Medical Image Analysis* **70**, 102030 (2021).

[7] Bayram, I. and Kamasak, M., "Directional total variation," *IEEE Signal Processing Letters* **19**, 781–784 (2012).

[8] Kongskov, R. D., Dong, Y., and Knudsen, K., "Directional total generalized variation regularization," *BIT Numerical Mathematics* (May 2019).

[9] Zhang, H. and Wang, Y., "Edge adaptive directional total variation," *The Journal of Engineering* **2013**(11), 61–62 (2013).

[10] Merveille, O., Naegel, B., Talbot, H., and Passat, N., "nD variational restoration of curvilinear structures with prior-based directional regularization," *IEEE Transactions on Image Processing* **28**(8), 3848–3859 (2019).

[11] Parisotto, S. and Schönlieb, C.-B., [*Total Directional Variation for Video Denoising*], Springer International Publishing (2019).

[12] Parisotto, S., Lellmann, J., Masnou, S., and Schönlieb, C.-B., "Higher-order total directional variation: Imaging applications," *SIAM Journal on Imaging Sciences* **13**(4), 2063–2104 (2020).

[13] Aujol, J.-F., Gilboa, G., Chan, T. F., and Osher, S., "Structure-texture image decomposition—modeling, algorithms, and parameter selection," *International Journal of Computer Vision* **67**, 111–136 (2006).

[14] Li, J., Miao, C., Shen, Z., Wang, G., and H.Yu, "Robust frame based x-ray ct reconstruction," *Journal of Computational Mathematics* **34**, 683–704 (2016).

[15] Savanier, M., Riddell, C., Trousset, Y., Chouzenoux, E., and Pesquet, J.-C., "Magnification-driven B-spline interpolation for cone-beam projection and backprojection," *Medical Physics* **48**(10), 6339–6361.

[16] Chambolle, A. and Dossal, C., "On the convergence of the iterates of "fista"," *Journal of Optimization Theory and Applications* **166**, 25 (2015).

[17] Combettes, P. L. and Pesquet, J.-C., "Proximal Splitting Methods in Signal Processing," in [*Fixed-Point Algorithms for Inverse Problems in Science and Engineering*], 185–212, Springer, New York, NY (2011).